Improved self-consistent and resolution-of-identity approximated Becke'05 density functional model of nondynamic electron correlation

Emil Proynov, Fenglai Liu, Yihan Shao, and Jing Kong

Citation: J. Chem. Phys. **136**, 034102 (2012); doi: 10.1063/1.3676726
View online: http://dx.doi.org/10.1063/1.3676726
View Table of Contents: http://jcp.aip.org/resource/1/JCPSA6/v136/i3
Published by the American Institute of Physics.

Improved self-consistent and resolution-of-identity approximated Becke'05 density functional model of nondynamic electron correlation

Emil Proynov,[1] Fenglai Liu,[2] Yihan Shao,[1] and Jing Kong[1,a)]
[1]*Q-Chem Inc., 5001 Baum Boulevard, Suite 690, Pittsburgh, Pennsylvania 15213, USA*
[2]*College of Chemistry, Beijing Normal University, Beijing 100875, China and Center for Computational Research, State University of New York at Buffalo, Buffalo, New York 14260, USA*

(Received 4 November 2011; accepted 22 December 2011; published online 17 January 2012)

In a recent letter [E. Proynov, Y. Shao, and J. Kong, Chem. Phys. Lett. **493**, 381 (2010)], Becke's B05 model of nondynamic electron correlation in density functional theory was implemented self-consistently with computational efficiency (the "SCF-RI-B05" scheme). Important modifications of the algorithm were done in order to make the self-consistency feasible. In the present work, we give a complete account of the SCF-RI-B05 algorithm, including all the formulae for the analytical representation of the B05 functional and for its self-consistent field (SCF) potential. The average performance of the SCF-RI-B05 method reported in the above letter was somewhat less accurate, compared to the original B05 implementation, mainly because the parameters of the original B05 model were optimized with post-local-spin-density calculations. In this work, we report improved atomization energies with SCF-RI-B05, based on a SCF re-optimization of its four linear parameters. The re-optimized SCF-RI-B05 scheme is validated also on reaction barriers, and on the subtle energetics of NO dimer, an exemplary system of strong nondynamic correlation. It yields both the binding energy and the singlet-triplet splitting of the NO dimer correctly, and close to the benchmarks reported in the literature. © *2012 American Institute of Physics*. [doi:10.1063/1.3676726]

I. INTRODUCTION

Systems with strong nondynamic (ND) electron correlation are a major challenge for density functional theory (DFT).[1–3] In polyatomic systems, this effect is in the core of the left-right correlation.[4] It becomes progressively stronger upon dissociating a covalent bond, "decoupling" the bond pair into two unpaired electrons. The left-right correlation keeps these unpaired electrons maximally apart, so that when one of them is near the "left atom," the other is near the "right atom," and vice versa. Generally, ND correlation arises from degeneracies and/or near-degeneracies of Hartree-Fock (HF), or Kohn-Sham (KS) occupied and virtual orbitals. More specific is the case of small-gap atomic systems where this effect can be particularly strong.[5] Various solid state phenomena, transition states of reactions, and transition-metal compounds manifest strong ND correlation. This has been a task mostly for multi-reference *ab initio* methods, while the accuracy of many DFT functionals here is often not enough. Multi-reference generalizations of the KS DFT scheme have been proposed with mixed success.[3,6] On the other hand, it has been argued that ND correlation should in principle be feasible even within a single-determinant KS approach.[1,2] The KS determinant is not supposed to approximate the exact ground state wave function but only to yield the exact electron density, if the exact functional would be known. All correlation effects should be taken care of by the exchange-correlation (XC) functional itself. A significant step along this line was the development of the exact-exchange based real-space correlation (RSC) methods B03 and B05.[1,7] Another RSC model that includes ND correlation with full exact exchange, the Perdew-Staroverov-Tao-Scuseria (PSTS) functional, was suggested later.[2] Other promising avenues of modeling the ND correlation are fledgling,[8–12] especially to mention here the fractional occupancy approach of Yang *et al*.[9,11,12] Recent improvements at random phase approximation level of the theory offer an interesting fully nonlocal DFT approach to ND correlation.[13]

The first B05 results reported by Becke[7] in a post-local-spin-density (LSD) manner were very accurate, especially concerning barriers of "difficult" reactions.[14] In order to reveal the full capacity of this new method, a self-consistent field (SCF) implementation is desirable.[15] In a recent letter,[16] we have reported an efficient SCF implementation of the B05 method, the SCF-RI-B05 scheme. To make the self-consistency feasible, some modifications of the method were suggested and discussed briefly in Ref. 16, dealing mainly with intrinsic discontinuities in the B05 functional and potential. The heavy computational cost of B05 was dramatically reduced based on resolution of identity (RI) technique. In this work, we present a complete account of the SCF-RI-B05 algorithm, including all the formulae of the analytical representation of the B05 functional (Sec. III and Appendix A) and of the corresponding potential (Secs. IV and V and Appendix B).

The preliminary assessment of the SCF-RI-B05 was done in Ref. 16 using the original B05 parameter values.[7] Some decrease of accuracy was found at SCF level compared to the original B05 results for atomization energies (AEs) and reaction barriers. The RI-B05 potential is different from the LSD potential, and so are the corresponding electron densities at convergence. Because of this, parameters that were optimized in a post-SCF fashion may not be the best choice for the SCF

a)Author to whom correspondence should be addressed. Electronic mail: jkong@q-chem.com.

implementation. The RI approximation itself may also cause some deviations from the original B05 setup. In this work, we present improved results with SCF-RI-B05 (Sec. VI) after rescaling the original B05 parameters within the SCF context and improving further the auxiliary basis set used in the RI fitting. The parameter re-optimization is only preliminary, without any dispersion terms added to the B05 functional so far, and using a relatively small training set of 39 atomization energies. The re-optimized SCF-RI-B05 scheme is further assessed using 69 atomization energy benchmarks from Truhlar's 105AE database,[17] energy barriers of 18 most difficult reactions of hydrogen abstraction from Truhlar's reactions database,[18] and the binding energy and singlet-triplet splitting of the NO dimer, an exemplary system of very strong nondynamic correlation.

II. THE B05 MODEL REVISITED

The B05 model was originally designed as an exact-exchange based RSC method. It involves a real-space analysis of the spin-resolved XC hole ($h^{xc}_{\sigma\sigma'}$). The latter is the non-classical component of the conditional pair probability given by the diagonal elements of the second order reduced density matrix (RDM-2), $\mathbf{\Gamma}_{\sigma\sigma'}$

$$P_{\sigma\sigma'}(1,2) = \frac{\mathbf{\Gamma}_{\sigma\sigma'}(1,2)}{\rho_\sigma(1)} = \rho_{\sigma'}(2) + h^{xc}_{\sigma\sigma'}(1,2), \quad (1)$$

where the electron coordinates ($\mathbf{r}_1, \mathbf{r}_2$) are denoted as "(1,2)", σ and σ' are spin indices, and $\rho_\sigma(1)$ is the electron density of spin σ at position $\mathbf{r}_1$. In B05, the XC hole is a sum of the exact-exchange hole and a model DFT correlation hole

$$h_{\mathrm{XC}\sigma\sigma'}(1,2) = \delta_{\sigma\sigma'} h^{\mathrm{ex}}_{\mathrm{X}\sigma}(1,2) + h^{\mathrm{DFT}}_{\mathrm{C}\sigma\sigma'}(1,2). \quad (2)$$

The exact-exchange hole can be readily expressed in terms of the occupied SCF molecular orbitals (MO) and the electron density[2]

$$h^{\mathrm{ex}}_{X\sigma}(1,2) = -\frac{1}{\rho_\sigma(1)} \sum_{i,j}^{\mathrm{occ}} \psi^*_{i\sigma}(1)\psi_{i\sigma}(2)\psi^*_{j\sigma}(2)\psi_{j\sigma}(1). \quad (3)$$

Regarding a finite system with boundary conditions at infinity, the following sum rule stems from the exact normalization of RDM-2

$$\int_{\infty^3} h^{\mathrm{ex}}_{X\sigma}(\mathbf{r}_1, \mathbf{r}_2) d\mathbf{r}_2 = -1, \qquad \text{at each reference point } \mathbf{r}_1. \quad (4)$$

For a given subdomain Ω of the system, a partial normalization of the exchange hole can be defined as[19]

$$\int_\Omega h^{\mathrm{ex}}_{X\sigma}(\mathbf{r}, \mathbf{s}) d\mathbf{s} = -N^\Omega_\sigma(\mathbf{r}), \quad N^\Omega_\sigma(\mathbf{r}) \le 1. \quad (5)$$

The closer the partial normalization $N^\Omega_\sigma(\mathbf{r})$ to 1 at a given point, the larger the depth of the exchange hole about that point (due to Eq. (4)) and the larger the portion of the hole that remains localized within Ω. In multicenter systems, the exact-exchange hole alone is artificially too delocalized even when a chemical bond is infinitely stretched. In wavefunction based multi-reference treatments, this spurious delocalization is cancelled out by a compensatory delocalization of the corresponding correlation hole.[4,13] The overall XC hole remains localized within a region of roughly atomic size[1] in non-periodic systems. When the exact exchange is combined with a model DFT correlation, such a complete cancellation does not occur. Pure-DFT correlation holes are fairly localized in nature. Local or semi-local DFT exchange holes are also localized by construction. This to some extent compensates for the lack of ND correlation at generalized-gradient approximation (GGA) and meta-GGA functional levels. However, the depth of the corresponding XC hole is not large enough, especially at stretched bond distances (by about a factor of two).[1,11] Becke has suggested a way to remedy this situation without using multi-reference wave functions.[1,7] Instead, the spherically averaged exchange hole of, say, spin α, $\bar{h}^{\mathrm{ex}}_{X\alpha}$, is deepened in a physically motivated manner by the exchange hole of opposite spin β and by a second order same-spin correction. This results in a new ND component ($\bar{h}^{nd}_{XC\alpha}$) of the spherically averaged XC hole

$$\bar{h}^{nd}_{XC\alpha}(\mathbf{r}, s) = \bar{h}^{\mathrm{ex}}_{X\alpha}(\mathbf{r}, s) + \left[f(\mathbf{r}) \bar{h}^{\mathrm{ex}}_{X\beta}(\mathbf{r}, s) + \bar{h}_{C\alpha\alpha}(\mathbf{r}, s) \right], \quad (6)$$

$$\bar{h}(\mathbf{r}, s) \equiv \frac{1}{4\pi} \iint h(\mathbf{r}, \mathbf{r}+\mathbf{s})\, d\omega_s, \;\; r \equiv r_1, \;\; s = |\, r_2 - r_1 \,|. \quad (7)$$

The second and the third term on the rhs of Eq. (6) are opposite-spin, and second-order same-spin components of the ND XC hole, respectively. The function $f(\mathbf{r})$ is a local "correlation factor." It is a complicated, position-dependent function, designed to measure the strength of opposite-spin ND correlation at each point.[1] The last term of Eq. (6) is a second-order same-spin correction to the ND correlation hole. It was introduced in B05 to improve the performance over the earlier B03 method for open-shell systems.[7] The corresponding energy contribution from these two terms stems from integrating the Coulomb potential of the ND part of the XC hole (the term in brackets in Eq. (6))

$$E^{\mathrm{nd\text{-}op}}_C = \frac{1}{2} \int f(\mathbf{r}) \left[\rho_\alpha(\mathbf{r}) U^{\mathrm{ex}}_{X\beta}(\mathbf{r}) + \rho_\beta(\mathbf{r}) U^{\mathrm{ex}}_{X\alpha}(\mathbf{r}) \right] d\mathbf{r}, \quad (8)$$

$$E^{\mathrm{nd\text{-}par}}_C = -\frac{1}{2} \sum_\sigma \int \rho_\sigma(\mathbf{r}) A_{\sigma\sigma}(\mathbf{r}) M^{(1)}_\sigma(\mathbf{r})\, d\mathbf{r}. \quad (9)$$

Here, $U^{\mathrm{ex}}_{X\sigma}$ is the spin-resolved Slater exact-exchange potential[1,7]

$$\mathrm{U}^{\mathrm{ex}}_{X\sigma}(\mathbf{r}) = 4\pi \int_{\infty^3} s\, ds\, \bar{h}^{\mathrm{ex}}_{X\sigma}(\mathbf{r}, s), \quad (10)$$

$A_{\sigma\sigma}$ are second-order same-spin correlation factors, and $M^{(1)}_\sigma$ is the first-order moment ($n = 1$ in Eq. (11)) of the Becke-Roussel (BR) relaxed exchange hole ($\bar{h}^{\mathrm{eff}}_{X\sigma}$) (Ref. 7)

$$M^{(n)}_\sigma(\mathbf{r}) = 4\pi \int_0^\infty s^{n+2} \left| \bar{h}^{\mathit{eff}}_{X\sigma}(\mathbf{r}, s) \right| ds. \quad (11)$$

The final form of the B05 energy functional reads

$$E^{\mathrm{B05}}_{\mathrm{XC}} = E^{\mathrm{HF}}_{\mathrm{X}} + a^{\mathrm{nd\text{-}opp}}_{\mathrm{c}} E^{\mathrm{nd\text{-}opp}}_{\mathrm{c}} + a^{\mathrm{nd\text{-}par}}_{\mathrm{c}} E^{\mathrm{nd\text{-}par}}_{\mathrm{c}} + a^{\mathrm{d\text{-}opp}}_{\mathrm{c}} E^{\mathrm{d\text{-}opp}}_{\mathrm{c}} + a^{\mathrm{d\text{-}par}}_{\mathrm{c}} E^{\mathrm{d\text{-}par}}_{\mathrm{c}}. \quad (12)$$

There are four linear parameters, $a^{\mathrm{i}}_{\mathrm{c}}$, in B05 and two nonlinear parameters in the dynamic correlation part, the last two terms

of Eq. (12). For the latter, Becke[20] uses his dynamic correlation functional BR94. It is an efficient meta-GGA correlation functional that was not given in fully analytic form. An accurate analytical interpolation of BR94 was reported later on in Ref. 21 and we use that form in the calculation of Eq. (12).

Finding suitable approximations of the correlation factors $f(\mathbf{r})$ and $A_{\sigma\sigma}(\mathbf{r})$ is primordial in this approach. Becke has suggested an interesting approximation of these, based on the normalization sum rule for the XC hole and physical arguments[1,7]

$$f(\mathbf{r}) = \min(f_\alpha(\mathbf{r}), f_\beta(\mathbf{r}), 1), \quad 0 \le f(\mathbf{r}) \le 1, \tag{13}$$

$$f_\sigma = \frac{1 - N_{X\sigma}^{\text{eff}}}{N_{X(-\sigma)}^{\text{eff}}}, \tag{14}$$

$$A_{\sigma\sigma} = \min(A_{1\sigma}, A_{2\sigma}), \quad A_{1\sigma} = \frac{1 - N_{X\sigma}^{\text{eff}} - f N_{X(-\sigma)}^{\text{eff}}}{M_\sigma^{(2)}},$$

$$A_{2\sigma} = \frac{D_\sigma}{3\rho_\sigma}, \ \text{(when } \sigma \equiv \alpha, (-\sigma) \equiv \beta \text{ and vice versa)}, \tag{15}$$

$$D_\sigma \equiv \tau_\sigma - \frac{1}{4}\frac{|\nabla\rho_\sigma|^2}{\rho_\sigma}, \tau_\sigma(\mathbf{r}) = \sum_i^{\text{occ}} |\nabla\psi_{i\sigma}(\mathbf{r})|^2, \tag{16}$$

where τ_σ is the (gauge-free) KS kinetic energy density as defined in Refs. 1 and 22, $M_\sigma^{(2)}$is the second-order moment of the Becke-Roussel relaxed exchange hole ($n = 2$ in Eq. (11)), and $N_{X\sigma}^{\text{eff}}$ is "relaxed" (or "effective") normalization of the exchange hole within a region of roughly atomic size. When the exact-exchange hole is relatively localized about a given reference point, $N_{X\sigma}^{\text{eff}}$ is close to 1 and the local correlation factor f, Eq. (13), is negligible. When the exact-exchange hole is more delocalized, $N_{X\sigma}^{\text{eff}}$ is smaller than 1 and f increases, indicating that the ND correlation correction is needed at such a reference point. The relaxed normalization, $N_{X\sigma}^{\text{eff}}$, is similar to the partial normalization defined by Eq. (5). However, the actual estimate of $N_{X\sigma}^{\text{eff}}$ is done in B05 in a different way, employing yet another model, the BR89 exchange hole model,[22] as an auxiliary tool. The original BR89 exchange hole[22] is normalized to -1, similar to Eq. (4). In B05, this normalization is relaxed by imposing the condition that the corresponding Slater potential of the BR89 exchange hole be equal to the exact-exchange Slater potential, $U_{X\sigma}^{\text{ex}}$, at each point. With this condition, the sum rule for the (spherically averaged) BR89 exchange hole integrates to values generally less than 1, even though the integration is kept over the whole space as in Eq. (4)

$$-4\pi \int_0^\infty \bar{h}_{X\sigma}^{\text{eff}}(\mathbf{r}; s)\, s^2\, ds = N_{X\sigma}^{\text{eff}} \le 1. \tag{17}$$

These values are then used as a measure of $N_{X\sigma}^{\text{eff}}(\mathbf{r})$ in Eq. (14). Enforcing the relaxing condition leads to a nonlinear algebraic equation for a certain dimensionless function, $x_\sigma(y_\sigma)$, that has to be solved at each point[7] (the B05 formulae here and further on are given in a rearranged, more convenient for differentiation form)

$$\frac{(x_\sigma - 2)}{x_\sigma^2}\left(e^{x_\sigma} - 1 - \frac{x_\sigma}{2}\right) = y_\sigma \equiv -\frac{3}{4\pi}\frac{Q_\sigma}{\rho_\sigma^2}U_{X\sigma}^{\text{ex}}, \tag{18}$$

where $(-Q_\sigma)$ is the curvature of the exact-exchange hole[1]

$$Q_\sigma(\mathbf{r}) = \frac{1}{6}[\nabla^2\rho_\sigma(\mathbf{r}) - 2D_\sigma(\mathbf{r})], \quad D_\sigma = \tau_\sigma - \frac{1}{4}\frac{|\nabla\rho_\sigma|^2}{\rho_\sigma}. \tag{19}$$

The relaxed exchange-hole normalization and the exchange-hole moments employ this $x(y)$ function extensively

$$N_{X\sigma}^{\text{eff}} = \left(\frac{2}{3}\right)^{3/2} \pi\, \rho_\sigma^{5/2} e^{x_\sigma}\left[\frac{(x_\sigma - 2)}{x_\sigma\, Q_\sigma}\right]^{3/2}, \tag{20}$$

$$M_\sigma^{(1)} = N_\sigma^{\text{eff}}\left(\frac{\rho_\sigma(x_\sigma - 2)}{6x_\sigma\, Q_{s\sigma}}\right)^{1/2}\left[x_\sigma + \frac{4}{x_\sigma} - \left(1 + \frac{4}{x_\sigma}\right)\mathrm{e}^{-x_\sigma}\right], \tag{21}$$

$$M_\sigma^{(2)} = N_\sigma^{\text{eff}}\frac{\rho_\sigma(x_\sigma - 2)}{6x_\sigma\, Q_\sigma}\left(x_\sigma^2 + 12\right). \tag{22}$$

In the original B03 and B05 models,[1,7] Eq. (18) was solved numerically at each point, and the function $x_\sigma(y_\sigma)$ was not given in analytic form. In Refs. 16 and 23, accurate analytic interpolations of x_σ (y_σ) were derived later on. Since the one used here was only briefly discussed in Ref. 16, we describe this procedure in more details in Sec. III.

In the context of Perdew's Jacob's ladder,[24] B05 belongs to the forth rung, or hyper-GGA functionals. Some exact coordinate scaling constraints have been found that such functionals should obey for the sake of rigor and robustness.[25] Among these, of particular importance is the exact-exchange scaling constraint in high-density limit[2,25]

$$\lim_{\lambda\to\infty} \frac{E_{\text{xc}}[\rho_\lambda]}{E_X^{\text{ex}}[\rho_\lambda]} = 1, \quad \rho_\lambda(\mathbf{r}) = \lambda^3\, \rho(\lambda\mathbf{r}). \tag{23}$$

Based on coordinate scaling arguments, it was pointed out[25] that the B05 functional generally violates the above constraint because it scales like exact exchange in high-density limit. Such a scaling is correct only at infinite bond lengths as in infinitely stretched H_2 for example.[25] There, an exact degeneracy develops, with the two opposite-spin electrons being either in a bonding, or in an anti-bonding spatial orbital.[25] Violating the constraint, Eq. (23) at finite bond lengths may seem a bad news for B05, but it also brings some good news. Such a scaling behavior allows to describe, in principle, the dissociation process continuously and without a symmetry breaking.[25] Other XC functionals require a spin-symmetry breaking to describe the bond dissociation. One should note that in "normal" systems (no degeneracy or near-degeneracy) the magnitude of the correlation factor $f(\mathbf{r})$, Eq. (13), is negligible (or vanishing) and the terms with improper coordinate scaling, Eqs. (8) and (9), have no influence.

III. ANALYTIC INTERPOLATION OF THE B05 CORRELATION FACTOR

Analytic interpolation of the B05 functional was first reported in Ref. 23. A somewhat different interpolation form that yields on average better accuracy was briefly outlined in Ref. 16. Here, we present this procedure in more detail. The

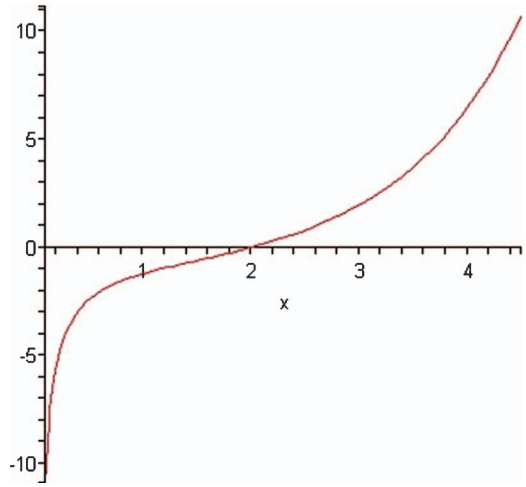

FIG. 1. The form of the starting function $y(x)$ of the interpolation task. This function has one single root, $y(x) = 0$ at $x = 2$.

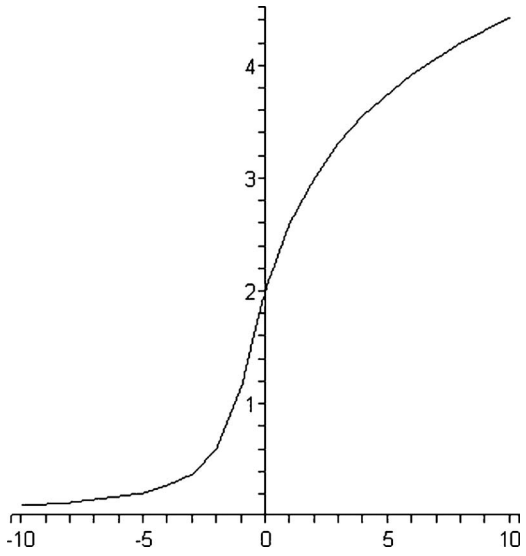

FIG. 2. The form of the yet unknown function $x(y)$ from numerical estimates.

object of interpolation is the dimensionless function, $x(y)$, entering the relaxed exchange-hole normalization, Eq. (20). The latter is obtained from the condition that the Slater potential of the relaxed exchange hole be equal to the exact-exchange Slater potential, which leads to the nonlinear algebraic equation for the function $x(y)$, Eq. (18), and to the expression for the relaxed normalization, Eq. (20). The reverse function, $y(x)$, is known from the outset and given by the left-hand side of Eq. (18), as shown in Fig. 1. It has the following asymptotic forms:

$$\lim_{x\to 0, x\geq 0} y(x) \to -\frac{1}{x} - \frac{1}{2} + \frac{1}{6}x \to -\infty, \tag{24}$$

$$\lim_{x\to 2} y(x) \to \left(\frac{e^2}{4} - \frac{1}{2}\right)(x-2) + \frac{3}{8}(x-2)^2 \to 0, \tag{25}$$

$$\lim_{x\to +\infty} y(x) \to \left(\frac{1}{x} - \frac{2}{x^2}\right) e^x - \frac{1}{2} + \frac{2}{x^2} \to +\infty. \tag{26}$$

The values of the unknown function $x(y)$ were first obtained numerically on a grid of points along the y axis, as depicted in Fig. 2. When y is negative, $x(y)$ takes values between 0 and 2. Since the Slater exchange potential is negative and the electron density is positive, negative y means, according to the rhs of Eq. (18), a positive curvature $(-Q_\sigma)$ of the exchange hole. Then the exact-exchange hole has a single minimum about the reference point, and the relaxed hole normalization is positively defined by virtue of Eq. (20). When the exchange hole curvature is negative (positive y and positive Q_σ), the function $x(y)$ is in the range $2 \leq x \leq +\infty$ and the relaxed normalization remains positive in this case as well. A negative hole curvature corresponds to a delocalized exchange hole with two distant minima on both sides of the reference point. To make the interpolation of $x(y)$ feasible, the y interval has been divided into three regions

$$\text{region I}\,(-\infty \leq y \leq 0.15),\ \text{region II}\,(-0.1 \leq y \leq 1001),$$
$$\text{and region III}\ (1000 \leq y \leq +\infty).$$

The small overlap between the regions facilitates the join between the interpolated pieces of $x(y)$. The join between regions I and II is at $y = 0$. This is an inflection point that delineates the cases of positive curvature of the exchange hole (negative y) from the cases of negative curvature (positive y). At the inflection point $y = 0$, $x(y) = 2$, the curvature of the relaxed exchange hole passes through zero. However, the relaxed normalization remains finite at that point, as we have verified it numerically (a finite 0/0 situation in Eq. (20)).

Regarding first region I ($-\infty \leq y \leq 0.15$), the function $x(y)$ takes values only between 0 and 2 for $y \leq 0$. Inverting the asymptotic expansion of $y(x)$, Eq. (25), about $x = 2$, $x \leq 2$, we obtain the following exact asymptotic form of $x(y)$, accurate in the range $-0.15 \leq y \leq 0$:

$$\lim_{y\to 0, y\leq 0} x(y) \approx \frac{8}{3} - \frac{e^2}{3} + \frac{1}{3}\sqrt{4 - 4e^2 + e^4 + 24y}\ . \tag{27}$$

From this asymptotic form, one can estimate the exact values of the first and the second derivatives of $x(y)$ about $y = 0$

$$\left.\frac{dx}{dy}\right|_{y=0} = 0.742245;$$
$$\left.\frac{d^2x}{dy^2}\right|_{y=0} = -0.306690\ \text{(exact estimates)}. \tag{28}$$

Using next a technique similar to that described in Ref. 21, we obtain the following interpolation of $x(y)$ that maintains high accuracy in the entire region I

$$x(y) = g(y)\frac{P_1(y)}{P_2(y)},\ g(y) = 2\frac{(2\arctan(a_1 y + a_2) + \pi)}{2\arctan(a_2) + \pi},$$
$$-\infty \leq y \leq 0.15, \tag{29}$$

$$P_1(y) = \sum_{i=0}^{5} c_i\, y^i; \quad P_2(y) = \sum_{i=0}^{5} b_i\, y^i, \tag{30}$$

where a_i, b_i, and c_i are interpolation coefficients given in Appendix A. Table I contains results of this interpolation. The

TABLE I. Results with the interpolation form designed for region I ($-\infty \le y \le 0.15$).

Values of y	Exact numerical values of $x(y)$	Interpolated values of $x(y)$	$x_{exact} - x_{interp}$
0.1	2.072693186	2.072391698	0.000301488
0.0	2.0000000000	2.000000000	0.000000000
−0.01	1.992562217	1.992570694	-8.48×10^{-6}
−0.1	1.924246541	1.924246541	3.10×10^{-10}
−0.3	1.763886032	1.763799872	8.62×10^{-5}
−0.5	1.593624260	1.593624260	0.000000000
−1.0	1.164014633	1.164014632	0.000000001
−2.0	0.610044631	0.610044631	0.000000000
−3.0	0.387784065	0.387784065	0.000000000
−8.0	0.132913594	0.132913594	0.000000000
−10.0	0.105059019	0.105059019	0.000000000
−40.0	0.0253137170	0.0253137287	-1.17×10^{-8}
−100.0	0.0100500810	0.0100500945	-1.35×10^{-8}
MAE[a]			6.38×10^{-6}
MAPE[a]			0.00051%

[a]The statistics is evaluated on a much larger set of values than the sample data in the table.

TABLE II. Results with the interpolation form designed for region II ($0 \le y \le 1000$).

Values of y	Exact numerical values of $x(y)$	$x(y)$ from our interpolation	x(exact) − x(interp)
−0.1	1.924246541	1.924246596	−0.000000055
0.0	2.0000000000	2.000000000	0.000000000
0.001	2.000742092	2.000742092	0.000000000
0.01	2.007407115	2.007407116	−0.000000001
0.1	2.072693186	2.072693186	0.000000000
0.5	2.334106024	2.334106024	0.000000000
1.0	2.604470724	2.604470724	0.000000000
2.0	3.016176365	3.016175226	1.14×10^{-6}
4.0	3.563036955	3.563037705	-7.50×10^{-7}
6.0	3.931439714	3.931439714	0.000000000
10.0	4.430554531	4.430554531	0.000000000
60.0	6.326557399	6.326557399	0.000000000
1000.	9.387175945	9.387175945	0.000000000
MAE[a]			3.67×10^{-6}
MAPE			6.7×10^{-6}%

[a]The statistics is evaluated on a much larger set of values than the sample data in the table.

mean absolute error (MAE) here is 6.38×10^{-6}, and the mean absolute percentage error (MAPE) is 0.00051%. The corresponding first derivatives with respect to y that are required for the derivation of the SCF potential read

$$\frac{dx}{dy} = \left(\frac{dg(y)}{dy}\right) \frac{P_1(y)}{P_2(y)} + g(y) \frac{d}{dy}\left[\frac{P_1(y)}{P_2(y)}\right], \quad (31)$$

$$\frac{dg(y)}{dy} = \frac{4a_1}{\left(1 + a_1^2 y^2 + 2a_1 a_2 y + a_2^2\right)(2\arctan(a_2) + \pi)}, \quad (32)$$

$$\frac{d}{dy}\left[\frac{P_1(y)}{P_2(y)}\right] = \frac{Q_1(y)}{P_2(y)^2}, \quad (33)$$

$$Q_1(y) = \sum_{i=0}^{9} q_i\, y^i. \quad (34)$$

The interpolation coefficients q_i in Eq. (34) are also given in Appendix A.

In region II ($-0.1 \le y \le 1001$), the function $x(y)$ equals 2 for $y = 0$, and is greater than 2, for $y>0$. The exact series expansion about $y = 0$, Eq. (27), is applicable also here up to $0 \le y \le 0.15$.

We have obtained an accurate fit of $x(y)$ in the entire region II as well, using Thiele interpolation technique of continuous fractions[21] (all the coefficients below are given in Appendix A)

$$x(y) = \frac{R_1(y)}{4R_2(y)}; \quad R_1(y) = \sum_{i=0}^{6} d_i\, y^i,$$

$$R_2(y) = \sum_{i=0}^{6} e_i\, y^i, \quad 0 \le y \le 1001. \quad (35)$$

Table II contains results with this interpolation in region II. The accuracy here is even higher (MAE = 3.67×10^{-6} and MAPE = 0.000067%), compared to the case of region I.

Equation (35) retains its accuracy up to $y \ge -0.1$, when penetrating back into region I. Thus, the two interpolation forms have an overlap domain ($-0.1 \le y \le +0.15$) around the border point $y = 0$, which facilitates the join. The first derivative of $x(y)$ in region II is given by

$$\frac{dx}{dy} = \frac{d}{dy}\left[\frac{R_1(y)}{4R_2(y)}\right] = \frac{Q_2(y)}{R_2(y)^2}, \quad Q_2(y) = \sum_{i=0}^{10} k_i\, y^i, \quad (36)$$

with the coefficients k_i given in Appendix A. The join between regions I and II is verified by comparing the first and the second derivatives of $x(y)$ at $y = 0$. The interpolation form Eq. (36) well reproduces the exact derivatives, Eq. (28)

$$\left.\frac{dx}{dy}\right|_{y=0} = 0.74224516;$$

$$\left.\frac{d^2x}{dy^2}\right|_{y=0} = -0.30669 \text{ (from the side of region II).} \quad (37)$$

With the interpolation in region I, Eq. (29), the derivatives are

$$\left.\frac{dx}{dy}\right|_{y=0} = 0.741258;$$

$$\left.\frac{d^2x}{dy^2}\right|_{y=0} = -0.33557 \text{ (from the side of region I).} \quad (38)$$

The first derivatives agree well comparing region I vs. region II. Some difference exists in the second derivatives, which is not of much importance since $x(y)$ is about linear in the vicinity of the border point $y = 0$.

In region III ($1000 \le y \le +\infty$), $x(y)$ is a slow varying function. We use there the interpolation form proposed first by Arbuznikov and Kaupp (Eq. (30) of Ref. 23), which we have found quite suitable for our region III. We have slightly

readjusted their parameter, ε, in order to conform better to the different partitioning of the y interval we use

$$x(y) = \ln(y)^{[1+\frac{1}{\ln(y)}]} + \frac{1.23767}{\ln(y)} + \frac{9.37587}{\ln(y)^2} - \frac{19.4777}{\ln(y)^3} + \frac{13.6816}{\ln(y)^4} - 0.078655. \quad (39)$$

The attained accuracy with this interpolation form (MAE = 0.0032 and MAPE = 0.029%) is about the same as the one reported in Ref. 23 within their range of $8 \le y \le +\infty$. The corresponding first derivative of $x(y)$ with this interpolation reads

$$\frac{dx}{dy} = \frac{\ln(y)^{[\frac{1}{\ln(y)}]}}{y}\left[-\frac{\ln(\ln(y))}{\ln(y)} + 1 + \frac{1}{\ln(y)}\right] + \frac{1}{y\,\ln(y)^2}\left[-\frac{54.7264}{\ln(y)^3} + \frac{58.4331}{\ln(y)^2} - \frac{18.75174}{\ln(y)} - 1.23767\right]. \quad (40)$$

The join between regions II and III at the border point $y = 1000$ is reasonable, comparing the values of the first and the second derivatives at that point

$$\left.\frac{dx}{dy}\right|_{y=1000} = 0.00095202;$$
$$\left.\frac{d^2x}{dy^2}\right|_{y=1000} = -0.000001266, \ \text{(region II)}, \quad (41)$$

$$\left.\frac{dx}{dy}\right|_{y=1000} = 0.0010836;$$
$$\left.\frac{d^2x}{dy^2}\right|_{y=1000} = -0.000001088, \ \text{(region III)}. \quad (42)$$

IV. DEALING WITH THE DISCONTINUITIES IN THE B05 FUNCTIONAL AND POTENTIAL

To implement a density functional self-consistently, the corresponding SCF potential must be well defined, which requires a functional differentiability. Analyses of the difficulties in differentiating the B05 functional have been given in Refs. 15, 16, and 26. A major problem here is that the f and $A_{\sigma\sigma}$ correlation factors, Eqs. (8) and (9), and their derivatives, are not continuous functions, especially regarding open-shell systems. The opposite-spin correlation factor $f(\mathbf{r})$ has two main sources of derivative discontinuity: the strict upper limit of 1, and the min() function used in its definition, Eq. (13). (Ref. 15). Physically, f should not be larger than 1, but in practice it may be so at some grid points due to the model character of the relaxed BR89 exchange hole and numerical inaccuracies. Enforcing the upper limit of f directly as in Eq. (13), introduces a derivative discontinuity. We suggested smoothening of this limit with a quadratic smoothing function to the first order when f deviates from 1 by a small difference δ

$$f_\sigma(\mathbf{r}) \leftarrow 1 - \frac{1}{4\delta}(f_\sigma(\mathbf{r}) - 1 - \delta)^2, \quad |f_\sigma(\mathbf{r}) - 1| \le \delta, \quad (43)$$

where values of $f_\sigma(\mathbf{r})$ larger than $f_\sigma(\mathbf{r})+\delta$ are capped to 1.0.

Note that the value of δ used here is $\delta = 0.05$, and not 0.005 as in Ref. 16. It is chosen based on more detailed numerical tests of SCF stability. The energy values are quite insensitive to the precise value of δ within a certain range, since this affects the correlation factor f at only a small fraction of grid points. With this modification, the opposite-spin correlation factor f becomes

$$f(\mathbf{r}) = \min(f_\alpha(\mathbf{r}), f_\beta(\mathbf{r})). \quad (44)$$

Strictly speaking, f should be positively defined, since the relaxed normalization $N_{X\sigma}^{\text{eff}}$ should not exceed 1.0 (see Eqs. (17) and (20)). In practice, $N_{X\sigma}^{\text{eff}}$ may exceed 1.0 occasionally at some points, due to numerical inaccuracies and model restrictions. In such cases, $f(\mathbf{r})$ becomes negative, due to Eq. (14). This was allowed (to some extent) in the B05 implementation of Refs. 1, 7, and 16, while it was strictly excluded in Ref. 15. We have found[16] that a strict enforcement of $N_{X\sigma}^{\text{eff}} \le 1$ leads to large deviations from the original B05 results. Fully relaxing this condition, however, leads also to deviations and problems with the SCF convergence in a number of cases.[15,26] Our numerical tests have shown that while $N_{X\sigma}^{\text{eff}}$ may exceed 1.0 for a number of points, it should not be larger than 2.0. With this in mind, we have introduced the condition $N_{X\sigma}^{\text{eff}} \le 2.0$, which has been confirmed with Becke in private communication. This condition is enforced in a smooth manner, similar to Eq. (43), with a smoothing parameter of 0.07. With this smoothened constraint, the side effects of having $f < 0$ at some points are subdued, while the original B05 relative energy benchmarks are still well reproduced.

Next, we need to deal with the impeding effect of the min() function in Eq. (44) on the differentiability of f. For this sake, we employ a Heaviside function of the form (the formulae here are slightly different from those reported in Ref. 16)

$$H(p;z) = \frac{1}{(1+e^{pz})}, \quad z \equiv \frac{(f_\alpha - f_\beta)}{\left(f_\alpha^2 + f_\beta^2\right)}. \quad (45)$$

The "smoothening" of the opposite-spin correlation factor f is then done by

$$f = (f_\alpha - f_\beta)H(p;z) + f_\beta. \quad (46)$$

This brings a second smoothening parameter, p, that controls the sharpness of the Heaviside function $H(\mathrm{p};z)$. A Heaviside function is used to smoothen the second-order correlation factors $A_{\sigma\sigma}$ as well

$$A_{\sigma\sigma} = t_\sigma\, H(q;t_\sigma) + A_{2\sigma}, \quad t_\sigma = A_{1\sigma} - A_{2\sigma}, \quad (47)$$

where $H(q;t_\sigma)$ has the same form as in Eq. (45) but with different arguments, $\mathrm{A}_{1\sigma}$ and $\mathrm{A}_{2\sigma}$ given by Eq. (15). The Heaviside parameters p and q were chosen via numerical tests of the SCF stability and convergence. The values used here and in Ref. 16 are $p = 115.0$ and $q = 120.0$. Small variations around

these values do not change noticeably the relative energies but can make a difference for the stability of SCF in some cases.

Having the relaxed BR exchange hole in an analytic form and the f and $A_{\sigma\sigma}$ factors smoothened, enable a feasible SCF-RI-B05 algorithm. The matrix elements of the SCF potential are obtained directly by differentiating each energy component in Eq. (12) with respect to the orbital coefficient matrix, $\boldsymbol{P}$, following the methodology of Refs. 27 and 28. This approach has an increasing popularity ("generalized Kohn-Sham" approach) due to its relative simplicity compared to the rigorous optimized effective potential method.[29] All the terms of the B05 potential matrix, $\boldsymbol{F}$, are readily available except those coming from the ND correlation components, Eqs. (8) and (9), μ and ν below are basis function indices

$$F_{\mu\nu}^{\mathrm{nd},\sigma} = \frac{\partial\left(E_{\mathrm{C}}^{\text{nd-op}} + E_{\mathrm{C}}^{\text{nd-par}}\right)}{\partial P_{\mu\nu}^{\sigma}} = \int \sum_i \frac{\partial\left(e_{\mathrm{c}}^{\text{nd-op}}(\mathbf{r}) + e_{\mathrm{c}}^{\text{nd-par}}(\mathbf{r})\right)}{\partial \xi_i} \frac{\partial \xi_i}{\partial P_{\mu\nu}^{\sigma}} d\mathbf{r},$$

$$P_{\mu\nu}^{\sigma} \equiv \sum_i^{\text{occ}} C_{i\mu}^{\sigma} C_{i\nu}^{\sigma}, \tag{48}$$

where $C_{i\mu}^{\sigma}$ are the (spin-resolved) MO coefficients of the occupied MOs, and $e_{\mathrm{c}}^{\text{nd-op}}$and $e_{\mathrm{c}}^{\text{nd-par}}$are the integral kernels in Eqs. (8) and (9), respectively. ξ_i runs over the B05 functional variables: ρ_σ, $(\nabla\rho_\sigma)^2$, $\nabla^2\rho_\sigma$, τ_σ, and $V_{X\sigma}^{\mathrm{ex}}$ $(\sigma = \alpha,\beta)$. $V_{X\sigma}^{\mathrm{ex}}$ here is the exact exchange energy density of spin σ related to the exact Slater potential, Eq. (10), and treated formally as another independent extra variable

$$V_{X\sigma}^{\mathrm{ex}}(\mathbf{r}) \equiv \rho_\sigma(\mathbf{r}) U_{X\sigma}^{\mathrm{ex}}(\mathbf{r}). \tag{49}$$

Consider first the opposite-spin ND correlation term rewritten in the form

$$E_C^{\text{nd-op}} = \frac{1}{2} a_c^{\text{nd-op}} \int f(\mathbf{r}) \left[\frac{\rho_\alpha(\mathbf{r})}{\rho_\beta(\mathbf{r})} V_{X\beta}^{\mathrm{ex}}(\mathbf{r}) + \frac{\rho_\beta(\mathbf{r})}{\rho_\alpha(\mathbf{r})} V_{X\alpha}^{\mathrm{ex}}(\mathbf{r})\right] d\mathbf{r}, \tag{50}$$

with $V_{X\sigma}^{\mathrm{ex}}$ as the exact exchange energy density, Eq. (49). Differentiating this expression with respect to the orbital coefficient matrix elements $P_{\mu\nu}^{\alpha}$ gives the following contribution to the KS potential matrix (see Eq. (48)):

$$F_{\mu\nu,\alpha}^{\text{nd-op}} = \frac{\partial E_{\mathrm{C}}^{\text{nd-op}}}{\partial P_{\mu\nu}^{\alpha}} = \frac{1}{2} a_c^{nd-op} \times \int \left\{ \begin{array}{l} \left(\sum_{\xi_\alpha} \frac{df}{d\xi_\alpha} \frac{\partial \xi_\alpha}{\partial P_{\mu\nu}^{\alpha}}\right)\left(\frac{\rho_\alpha}{\rho_\beta} V_{X\beta}^{\mathrm{ex}} + \frac{\rho_\beta}{\rho_\alpha} V_{X\alpha}^{\mathrm{ex}}\right) \\ + f\left(\frac{V_X^{\mathrm{ex},\beta}}{\rho_\beta} - \frac{\rho_\beta}{\rho_\alpha^2} V_X^{\mathrm{HF},\alpha}\right) \frac{\partial \rho_\alpha}{\partial P_{\mu\nu}^{\alpha}} + f \frac{\rho_\beta}{\rho_\alpha} \frac{\partial V_X^{\mathrm{ex},\alpha}}{\partial P_{\mu\nu}^{\alpha}} \end{array} \right\} d\mathbf{r}, \tag{51}$$

where ξ runs over all independent functional variables. In a similar manner, the contribution from the same-spin ND correlation, Eq. (9), to the KS potential matrix is obtained as

$$F_{\mu\nu,\alpha}^{\text{nd-par}} = \frac{\partial E_C^{\text{nd-par}}}{\partial P_{\mu\nu}^{\alpha}} = -\frac{1}{2} \int \left[\frac{\partial \rho_\alpha}{\partial P_{\mu\nu}^{\alpha}} A_{\alpha\alpha} M_\alpha^{(1)} + \rho_\alpha \sum_{\xi_\alpha} \frac{d\left(A_{\alpha\alpha} M_\alpha^{(1)}\right)}{d\xi_\alpha} \frac{\partial \xi_\alpha}{\partial P_{\mu\nu}^{\alpha}} + \rho_\beta M_\beta^{(1)} \sum_{\xi_\alpha} \frac{dA_{\beta\beta}}{d\xi_\alpha} \frac{\partial \xi_\alpha}{\partial P_{\mu\nu}^{\alpha}}\right] d\mathbf{r}. \tag{52}$$

The derivatives of the functions f, $A_{\sigma\sigma}$, and $M_\sigma^{(1)}$ with respect to their variables are next obtained by employing the chain rule and the analytic interpolation formulae, Eqs. (29)–(40). The final expressions of all derivatives that are needed to evaluate Eqs. (48)–(52) are given in Appendix B. In implementing these expressions, special care must be taken to avoid occasions of overflow at some points. The complexity of the B05 SCF potential demands somewhat more stringent numerical cutoffs. For example, the contribution from grid points with electron density smaller than 10^{-8} is plagued with larger numerical inaccuracies and must be omitted.

V. EXACT EXCHANGE ENERGY DENSITY AND THE RI APPROXIMATION

The exact exchange energy density can be written in the following convenient form:

$$V_{X\sigma}^{\mathrm{ex}}(\mathbf{r}) = -\sum_{i,j}^{\text{occ}} \rho_{ij}^{\sigma}(\mathbf{r}) v_{ij\sigma}(\mathbf{r}), \tag{53}$$

where ρ_{ij}^{σ} is the density of the MO pair $|\mathrm{i}_\sigma \mathrm{j}_\sigma\rangle$ and $v_{ij\sigma}$ is the corresponding Coulomb potential

$$v_{ij\sigma}(\mathbf{r}) \equiv \int \frac{\rho_{ij}^{\sigma}(\mathbf{r}')}{|\mathbf{r} - \mathbf{r}'|} d\mathbf{r}'. \tag{54}$$

There are at least two ways of evaluating $V_{X\sigma}^{\mathrm{ex}}$ at each grid point. One way is to implement Eq. (53) as it is, after obtaining $v_{ij\sigma}$ first. The latter can be done by solving the Poisson equation at each grid point[1]

$$-\frac{1}{4\pi} \nabla^2 v_{ij}(\mathbf{r}) = \rho_{ij}(\mathbf{r}). \tag{55}$$

Solving this equation costs as $\mathrm{O}(N_G^2)$, where N_G is the number of grid points per MO pair. The total cost for all MO pairs then scales as $\mathrm{O}(N_O^2 N_G^2)$, where N_O is the number of occupied MOs. The main cost of this approach is the solution of the Poisson equation. Another popular approach is to expand the MOs, ψ_i and ψ_j, in atomic orbital (AO) basis $\{\phi_\mu\}$

$$V_{X\sigma}^{\mathrm{ex}}(\mathbf{r}) = -\sum_{\mu,\nu,\lambda,\omega} P_{\mu\nu}^{\sigma} P_{\lambda\omega}^{\sigma} \phi_\mu(\mathbf{r}) \phi_\lambda(\mathbf{r}) v_{\nu\omega}(\mathbf{r}), \tag{56}$$

where $\boldsymbol{P}^{\sigma}$ is the spin-resolved MO coefficient matrix and $v_{\nu\omega}$ is the Coulomb potential of the basis-function pair (BFP), $\phi_\nu\phi_\omega$. The Coulomb potential, $v_{\nu\omega}$, can be evaluated analytically at each grid point, using known recursive relationships. The total cost then becomes $\mathrm{O}(N_G N_B^4)$, where N_B is the number of basis functions. Still, this is a very high cost, since the exact exchange energy density is required at each grid point. To calculate $V_{X\sigma}^{\mathrm{ex}}$ at each point by Eq. (56) requires looping over four AO indices. This has a computational cost similar to that of calculating the total HF energy analytically. There are thousands of grid points for each atom, making the whole

scheme prohibitively expensive. In Ref. 16, we proposed a cost-effective alternative of calculating $V_{X\sigma}^{\rm ex}$, based on a specific use of the RI approximation.[30] Here, we present this technique in more details. We first expand each given BFP $\phi_\nu\phi_\omega$ as a linear combination of auxiliary basis functions X_m of Gaussian type

$$\phi_\mu(\mathbf{r})\phi_\nu(\mathbf{r}) \approx \sum_m C_m^{\mu\nu} X_m(\mathbf{r}) \,, \tag{57}$$

where $C_m^{\mu\nu}$ are the RI fitting coefficients. To apply the RI technique to the exact exchange energy density calculation, we next expand each MO pair density, ρ_{ij}, as a linear combination of auxiliary basis functions

$$\rho_{ij}^\sigma(\mathbf{r}) \approx \sum_{\mu,\nu,m} C_{i\mu}^\sigma C_{j\nu}^\sigma C_m^{\mu\nu} X_m(\mathbf{r}) \equiv \sum_m C_m^{ij,\sigma} X_m(\mathbf{r}) \,. \tag{58}$$

This leads to

$$V_{X\sigma}^{\rm ex}(\mathbf{r}) \approx -\sum_{m,n} X_m(\mathbf{r}) \int \frac{1}{|\mathbf{r}-\mathbf{r}'|} X_n(\mathbf{r}')d\mathbf{r}' \times \sum_{i,j}^{\rm occ} C_m^{ij,\sigma} C_n^{ij,\sigma} \equiv -\sum_{m,n} V_{mn}(\mathbf{r}) B_{mn}^\sigma \,. \tag{59}$$

B_{mn}^σ is also a function of $\boldsymbol{P}^\sigma$ through Eqs. (48), (57), and (58) as $\sum_{\mu,\nu,\lambda,\eta} P_{\mu\nu}^\sigma P_{\lambda\eta}^\sigma C_m^{\mu\lambda} C_n^{\nu\eta}$. To evaluate this expression, one first forms the matrices $V_{mn}(\mathbf{r})$ and B_{mn}^σ, and the exact exchange energy density is then the dot product of the two. Compared to the exact formula, Eq. (56), the calculation of $V_{mn}(\mathbf{r})$ now involves only two atom-centered indices associated with each grid point instead of four, which reduces significantly the cost. The evaluation of B_{mn}^σ is a linear algebra operation and can be done out of the loop over grid points. Note that the matrix $\{V_{mn}\}$ defined by Eq. (59) is not symmetric, and needs to be corrected as

$$V_{mn} = \frac{1}{2}(V_{mn} + V_{nm}). \tag{60}$$

As we have shown in Ref. 16, the computational efficiency of B05 improves dramatically with our RI implementation. For example, the cost of computing one SCF iteration of benzene with RI-B05 is about 100 times smaller than the cost for the same without RI. Table III presents examples of time-cost differences for B05 calculations with and without RI.

TABLE III. Timing of SCF-RI-B05: central processing unit time for one iteration in minutes, all calculations are done with a development version of Q-Chem using G3LARGE basis set (128,194) grid, and an enlarged auxiliary basis set and the same computational environment. The timing of the popular hybrid functional B3LYP is included for comparison.

Method	Pyrrole	Benzene	$(\text{Butane})_2$	Iso-octane	naphthalene
B05	447.4	1154.6	22326.4	12669.3	7887.7
RI-B05	8.1	12.1	56.7	52.8	36.9
B3LYP	0.7	1.2	5.9	7.0	4.8

VI. RESULTS AND DISCUSSIONS

In this section, we discuss new assessment data for SCF-RI-B05, after readjusting the original B05 parameters to match better the SCF implementation. All calculations are carried out with a development version of Q-Chem program.[31] The basis set used in all tests is G3LARGE.[32] Unpruned grid composed of 128 radial points and 302 angular points per atomic region is employed, unless mentioned otherwise. Converged HF electron density is used as an initial guess for SCF-RI-B05, which greatly stabilizes the convergence. Converged LSD output can also be used as an initial guess here, but we have found that the SCF-RI-B05 is slightly more efficient with a HF initial guess. An accurate RI calculation of the exact exchange energy density requires exceptionally large and accurate auxiliary basis set. For the calculations reported in Ref. 16, a new auxiliary bases set was developed based on the rimp2-cc-pVTZ auxiliary basis patterns developed in Ref. 30. The present calculations are done with a more extended version of our previous cc-pVTZ type auxiliary basis set, using an even-tempered technique for augmenting the basis. The RI error in reproducing the exact exchange energy is typically about 10^{-7} to 10^{-5} a.u. The converged SCF-RI-B05 energies differ from the original post-LSD B05 energy, generally by about 0.005 to 0.01 Hartrees. Preliminary assessment of RI-B05 (with and without SCF) was done in Ref. 16 on atomization energies and reaction barriers, without changing the original B05 parameters. The MAE for atomization energies has increased by about 1.2 kcal/mol and the MAE for reaction barriers has increased by about 0.6 kcal/mol with SCF-RI-B05 compared to the original (post-LSD) B05 performance. This situation was quite unsatisfactory, and we have attempted a readjustment of the four linear parameters in B05, looping over the rapid "LAP" test set of 39 benchmark atomization energies.[16,27] In addition to this, we kept track on the binding energy of the NO dimer during the parameter variations, which is one of the most notorious systems with strong ND correlation. The following parameter values were found to provide a balanced improvement of the RI-B05 at SCF level:

$$a_{\rm c}^{\text{nd-opp}} = 0.5260; \quad a_{\rm c}^{\text{nd-par}} = 0.6467; \quad a_{\rm c}^{\text{d-opp}} = 1.0754; \quad \text{and} \quad a_{\rm c}^{\text{d-par}} = 1.130 \,.$$

In comparison, the original B05 values of these parameters were[7]

$$a_{\rm c}^{\text{nd-opp}} = 0.514, \quad a_{\rm c}^{\text{nd-par}} = 0.651, \quad a_{\rm c}^{\text{d-opp}} = 1.075, \quad \text{and} \quad a_{\rm c}^{\text{d-par}} = 1.113 \,.$$

Our new parameter values are not much different from the original B05 values. The largest deviation here is about 2.3% for $a_{\rm c}^{\text{nd-op}}$. The so re-optimized RI-B05 scheme is next tested on the AE (at fixed geometry) of a subset of 69 molecules from the Truhlar 105AE database,[17,18] for which we have found reliable geometry benchmarks. The complete list of our test set and the AE results with the present SCF-RI-B05 are listed in Appendix C. Table IV contains the statistics of the AE performance of several functionals. It is seen that the parameter readjustment was worth the effort, for AEs at

TABLE IV. Mean absolute errors for atomization energies D_e (kcal/mol) on the 69AE test set of functional assessment.

	MAE for D_e [a]		
XC	26 diatomic	43 polyatomic	All 69 molecules
B3LYP	2.24	3.44	2.99
B3tLap	2.41	2.34	2.37
Post-LSD-RI-B05	2.71	2.14	2.35
SCF-RI-B05[b]	3.06	4.06	3.68
SCF-RI-B05[c]	2.56	2.18	2.32
M06-2X	1.56	2.23	1.98

[a]The reference D_e values are from Refs. 18 and 35.
[b]SCF-RI-B05 calculations using the original B05 parameter values.
[c]SCF-RI-B05 calculations using the new parameter values of this work.

least: the MAE of the SCF-RI-B05 performance drops from 3.68 kcal/mol to 2.32 kcal/mol with the new parameters. This is a slight improvement over the performance of the post-LSD-B05 with MAE of 2.35 kcal/mol on the same test set. About the same is the performance here of the recent hybrid scheme B3tLap (Ref. 33) with MAE of 2.37 kcal/mol. B3LYP has the biggest MAE on this test set (2.99 kcal/mol). The multi-parameter functional M06-2X has the smallest MAE (1.98 kcal/mol) here. The considered 69 benchmark molecules are a part of the training set for M06-2X.[34]

An accurate prediction of reaction barriers requires an adequate description of the ND correlation, because the transition states are structures with stretched chemical bonds.[14] In Ref. 16, the barriers of 18 most "difficult" reactions from the Truhlar database were calculated with several methods. Here, we present again some of this data for comparison (Table V), together with the new SCF-RI-B05 results. The post-LSD RI-B05 results remain with the smallest MAE here (1.3 kcal/mol), which is slightly better than the MAE of 1.5 kcal/mol of the multi-parameter M06-2X functional[35] that was optimized particularly for reaction barriers. The training set used to optimize the four parameters in B05 does not include reaction barriers. The present SCF-RI-B05 scheme leads to some increase of MAE for the reaction barriers (MAE = 1.8 kcal/mol), compared to the post-LSD RI-B05, but it is still an accurate performance.

Special attention deserves the subtle case of *cis* NO dimer (ONNO). This is a system with a notoriously strong

TABLE VI. Singlet-triplet split Δ_{T-S} (kcal/mol), dimerization energy D_e (kcal/mol, basis-set superposition error (BSSE) corrected), and geometry (R_{N-N} and R_{N-O} in Å, ∠NNO in degree) of *cis* NO dimer ONNO.

	B3LYP	BP	B3tLap	M06-2X	SCF-RI-B05 [a]	MRCI	Expt[d]
Δ_{T-S}	−2.3	−4.9	+0.3	+4.0	+6.6	+6.3[c]	
D_e	−3.1	9.7	−0.9	−6.7	+5.3	3.3[b]	2.9–3.3
R_{N-N}	1.972	2.045	1.982	1.828	1.994	2.28[b]	2.263
R_{N-O}	1.147	1.160	1.149	1.143	1.149	1.149[b]	1.152
∠NNO	101.5	99.9	102.4	104.4	101.3	96.1[b]	97.17

[a]SCF-RI-B05 result of the present work at optimized "by hand" geometry of the NO dimer.
[b]Results of Ref. 37.
[c]$\Delta_{T-S} = E(^3B_1) - E(^1A_1)$ from Ref. 38. Positive Δ_{T-S} means the singlet is more stable.
[d]Data from Refs. 41 and 42.

ND correlation that is very difficult to describe quantitatively. The experiment indicates a rather weak binding energy (D_e) of about 2.9 kcal/mol to 3.3 kcal/mol,[36] the singlet *cis* ONNO configuration being the most stable. This has been confirmed by several high-quality multi-reference studies.[37–40] The closest triplet state, $^3B_1$, is about 6.3 kcal/mol higher.[38] Wave function methods based on single HF reference such as MP2, and even coupled-cluster method with singles, doubles, and perturbative triples (CCSD(T)), fail to predict the correct energy ordering here.[36,40] The early DFT studies[36] yielded a triplet ground state, in contradiction to experiment and multi-reference configuration interaction (MRCI). Table VI contains some of the results reported in Ref. 16, together with our new estimates with the present SCF-RI-B05 scheme. The singlet-triplet split is calculated at the optimized geometries for each functional. The split obtained with the present SCF-RI-B05 scheme is +6.6 kcal/mol, which is the closest one can get to the MRCI benchmark of +6.3 kcal/mol. No other functional gives a split any close to the benchmark here. Some of them (B3LYP, BP) predict the triplet lower than the singlet. Considering the binding energy, the present SCF-RI-B05 estimate of +5.3 kcal/mol is in relatively good agreement with the MRCI value of +3.3 kcal/mol, given the fact that no other functional gives any binding of the dimer whatsoever, except the GGA BP. The latter yields a binding of +9.7 kcal/mol which is too big, and even bigger is the spu-

TABLE V. The classical barriers for 18 "difficult" reactions from Truhlar's database (f = forward, r = reverse).

Reaction V_f; V_r	RI-B05[a]	SCF-RI-B05[b]	M06-2X	B3tLap	B3LYP	Reference[c]
$H + HCl \leftrightarrow H_2 + Cl$	5.8; 9.2	4.3; 7.0	4.3; 6.8	3.8; 6.3	−0.7; 4.4	5.7; 8.7
$H + HCl \leftrightarrow HCl + H$	17.7	17.8	18.1	16.3	12.7	18.0
$H + OH \leftrightarrow H_2 + O$	7.8; 12.8	6.6; 10.5	9.2; 11.7	7.3; 9.0	4.0; 6.2	10.7; 13.1
$F + H_2 \leftrightarrow HF + H$	3.0; 35.1	−2.2; 30.9	1.0; 31.5	−3.6; 26.8	−5.6; 23.2	1.8; 33.4
$H + H_2 \leftrightarrow H_2 + H$	10.4	8.6	11.6	7.5	4.3	9.6
$OH + H_2 \leftrightarrow H + H_2O$	5.6; 21.3	2.8; 19.0	4.6; 20.8	3.1; 17.4	0.8; 13.3	5.1; 21.2
$OH + NH_3 \leftrightarrow H_2O + NH_2$	3.2; 13.2	1.8; 11.8	2.2; 11.8	−0.5; 8.9	−2.3; 7.2	3.2; 12.7
$H + H_2S \leftrightarrow HS + H_2$	3.1; 17.9	1.9; 15.9	4.5; 18.1	2.6; 16.5	−0.4; 15.9	3.5; 17.3
$O + HCl \leftrightarrow OH + Cl$	15.8; 14.2	8.4; 7.0	7.3; 7.1	4.2; 5.0	1.5; 4.4	9.8; 10.4
$H + CH_3OH \leftrightarrow H_2 + CH_2OH$	9.8; 15.7	8.1; 13.4	10.1; 15.8	6.7; 14.1	3.7; 13.2	7.3; 13.8
MAE on 18 reactions	1.3	1.8	1.5	2.9	5.6	

[a]Results from post-LSD RI-B05 of Ref. 16.
[b]SCF-RI-B05 results of the present work using the new parameters and HF guess.
[c]Best available reference values from the Truhlar's online database (http://comp.chem.umn.edu/database).

rious binding of the triplet state with BP (+14.6 kcal/mol). It is clear that the subtle electronic structure in ONNO can be described only with a DFT method that includes explicitly ND correlation in a physically sound manner.

VII. CONCLUSIONS

Combining a 100% exact exchange with a proper correlation functional has been a long-standing problem in Kohn-Sham DFT. The B03 and B05 RSC schemes by Becke are a breakthrough along this line. Unfortunately, their original formulation is prohibitively expensive. In a recent study,[16] the B05 functional was implemented in a fully analytic, continuous form that allows a consistent and efficient SCF implementation. Here, we presented a full account of this algorithm in detail and list all the formulae necessary for the analytical representation of the functional and its potential. We have noted that the accuracy of the RI-B05 results at SCF level somewhat deteriorates when the four linear parameters are kept at their original post-LSD values. In this work, we report a reoptimized SCF-RI-B05 scheme that leads to a considerably improved atomization energies, compared to the SCF-B05 results previously reported.[16] This comes with no improvement so far for reaction barriers, but the performance there remains very good as well. The SCF-RI-B05 scheme offers an accurate description of the subtle energy features of the NO dimer, an exemplary system of strong ND correlation. We present in full details the algorithm behind the SCF-RI-B05 scheme, including all the formulae necessary to program the corresponding SCF potential.

ACKNOWLEDGMENTS

The work is supported by a grant from National Institute of Health (GM081928). The authors wish to thank Dr. Zhengting Gan for technical assistance. J.K. and E.P. wish to thank Dr. Axel Becke for helpful discussions.

APPENDIX A: VALUES OF ALL THE INTERPOLATION COEFFICIENTS REFERRED TO IN SEC. III

The two interpolation coefficients in Eq. (29) read

$a_1 = 0.9301841768238374$ and $a_2 = 0.5485569431916153$.

The values of the coefficients c_i, b_i entering Eq. (30) read

$c_0 = -5.968528012907202$; $c_1 = -2.183747742603848$; $c_2 = -4.985886441243756$; $c_3 = -1.134161212063683$; $c_4 = -1.692142642619975$; and $c_5 = 0.570895953834689$;

$b_0 = -5.968528013066088$; $b_1 = -2.030780232084790$; $b_2 = -4.679675048001286$; $b_3 = -1.118849057754117$; $b_4 = -1.808705503402923$; and $b_5 = 0.592264821617529$.

The values of the coefficients d_i, e_i entering Eq. (35) read

$d_0 = 26.88413661379433$; $d_1 = 46.96693640414017$; $d_2 = 33.17800151829805$; $d_3 = 9.940088877152307$; $d_4 = 0.8786661786414733$; $d_5 = 0.01643722176146135$; and $d_6 = 3.40424464772731\ 10^{-5}$.

$e_0 = 3.36051707672429$; $e_1 = 4.623703278485152$; $e_2 = 2.68894984040501$; $e_3 = 0.6007166968496472$; $e_4 = 0.0392204000640807$; $e_5 = 0.0005438465669613952$; and $e_6 = 7.8437439010087\ 10^{-7.}$

The values of the coefficients q_i and k_i entering Eq. (34) and (36), respectively, read

$q_0 = 0.9129908719446399$; $q_1 = 3.655262558462426$; $q_2 = 0.1801828684494572$; $q_3 = -3.062938667772561$; $q_4 = -1.173405187745653$; $q_5 = -1.662674088158794$; $q_6 = 0.6859613559654089$; $q_7 = 0.06595477584967326$; $q_8 = -0.03038609318852905$; and $q_9 = -7.717661265301923\ 10^{-16}$.

$k_0 = 8.382230306773296$; $k_1 = 19.60257290836815$; $k_2 = 19.71894106502952$; $k_3 = 10.77146542063455$; $k_4 = 3.415698370189622$; $k_5 = 0.5813153924917321$; $k_6 = 0.05426084060061605$; $k_7 = 2.299629631716270\ 10^{-3}$; $k_8 = 5.119354330427682\ 10^{-5}$; $k_9 = 3.229775610122730\ 10^{-7}$; and $k_{10} = 1.405232963383258\ 10^{-9}$.

APPENDIX B: SUMMARY OF ALL ADDITIONAL DERIVATIVES REQUIRED FOR THE SCF POTENTIAL

Below is a summary of all the derivatives involved in Eqs. (48), (51), and (52). Regarding first the opposite-spin correlation factor f, differentiating Eq. (46) with respect to a functional variable, ξ_α, gives

$$\frac{df}{d\xi_\alpha} = \frac{\partial f_\beta}{\partial \xi_\alpha} + \left(\frac{\partial f_\alpha}{\partial \xi_\alpha} - \frac{\partial f_\beta}{\partial \xi_\alpha}\right) H(p;z) - \left[G_\alpha \frac{\partial f_\beta}{\partial \xi_\alpha} + G_\beta \frac{\partial f_\alpha}{\partial \xi_\alpha}\right] Q(p;z), \quad \text{(B1)}$$

where H(p;z) is given by Eq. (45)

$$Q(p;z) = p\,z\,H(p;z)^2 \exp(pz)\left(f_\alpha^2 + f_\beta^2\right)^{-1}, \quad \text{(B2)}$$

$$G_\alpha = f_\beta^2 - f_\alpha^2 - 2 f_\alpha f_\beta$$

$$G_\beta = f_\beta^2 - f_\alpha^2 + 2 f_\alpha f_\beta,$$

$$\frac{df}{d\xi_\beta} = \frac{\partial f_\beta}{\partial \xi_\beta} + \left(\frac{\partial f_\alpha}{\partial \xi_\beta} - \frac{\partial f_\beta}{\partial \xi_\beta}\right) H(p;z) - \left[G_\alpha \frac{\partial f_\beta}{\partial \xi_\beta} + G_\beta \frac{\partial f_\alpha}{\partial \xi_\beta}\right] Q(p;z). \quad \text{(B3)}$$

Next, differentiating the expression of the same-spin correlation factors, Eq. (47), gives

$$\frac{dA_{\sigma\sigma}}{d\xi_\sigma} = \frac{\partial A_{2\sigma}}{\partial \xi_\sigma} + \left(\frac{\partial A_{1\sigma}}{\partial \xi_\sigma} - \frac{\partial A_{2\sigma}}{\partial \xi_\sigma}\right) J_\sigma(q;t_\sigma),$$

$$\frac{\partial A_{2\sigma}}{\partial \xi_\sigma} = 0 \text{ for } \xi_\sigma = \nabla^2\rho_\sigma \text{ and } V^{\text{ex}}_{X\sigma}, \tag{B4}$$

$$J_\sigma(q;t_\sigma) = H(q;t_\sigma) - qt_\sigma H(q;t_\sigma)^2 \exp(qt_\sigma), \tag{B5}$$

$$\frac{dA_{\alpha\alpha}}{d\xi_\beta} = \frac{\partial A_{1\alpha}}{\partial \xi_\beta} J_\alpha, \quad \frac{dA_{\beta\beta}}{d\xi_\alpha} = \frac{\partial A_{1\beta}}{\partial \xi_\alpha} J_\beta. \tag{B6}$$

The partial derivatives of f_α, f_β entering Eq. (B3) are obtained by differentiating their smoothened forms, Eq. (43), in conjunction with Eq. (14)

$$\frac{\partial f_\sigma}{\partial \xi_\sigma} = -S_{f\sigma} \frac{dN^{\text{eff}}_{X\sigma}}{d\xi_\sigma} \left(N^{\text{eff}}_{X(-\sigma)}\right)^{-1}, \tag{B7}$$

$$\frac{\partial f_\alpha}{\partial \xi_\beta} = -S_{f\alpha} \frac{dN^{\text{eff}}_{X\beta}}{d\xi_\beta} \frac{\left(1 - N^{\text{eff}}_{X\alpha}\right)}{\left(N^{\text{eff}}_{X\beta}\right)^2}, \tag{B8}$$

$$S_{f\sigma} = \begin{cases} 1, & g_{c\sigma} \le (1-\delta) \\ -\dfrac{(g_{c\sigma} - 1 - \delta)}{2\delta}, & (1-\delta) < g_{c\sigma} < (1+\delta), \\ 0, & g_{c\sigma} \ge (1+\delta) \end{cases} \qquad g_{c\sigma} = \frac{1 - N^{\text{eff}}_{X\sigma}}{N^{\text{eff}}_{X(-\sigma)}}. \tag{B9}$$

Note that even for closed-shell systems one must start with the above spin-resolved derivatives before equalizing the spin-up and spin-down components. This was noted first in Ref. 15.

More complicated are the derivatives of the relaxed exchange hole normalization obtained by differentiating Eq. (20). First, consider the derivative over the electron density using the chain rule

$$\frac{dN^{\text{eff}}_{X\sigma}}{d\rho_\sigma} = \frac{\partial N^{\text{eff}}_{X\sigma}}{\partial \rho_\sigma} + \frac{\partial N^{\text{eff}}_{X\sigma}}{\partial x_\sigma}\frac{dx_\sigma}{dy_\sigma}\frac{\partial y_\sigma}{\partial \rho_\sigma} + \frac{\partial N^{\text{eff}}_{X\sigma}}{\partial Q_\sigma}\frac{\partial Q_\sigma}{\partial \rho_\sigma}, \tag{B10}$$

where Q_σ is given by Eq. (19)

$$\frac{\partial N^{\text{eff}}_{X\sigma}}{\partial \rho_\sigma} = S_{N\sigma}\frac{5}{2\rho_\sigma}\left(\frac{2}{3}\right)^{3/2} \pi\, \rho_\sigma^{5/2} e^{x_\sigma} \left[\frac{(x_\sigma - 2)}{x_\sigma\, Q_\sigma}\right]^{3/2}, \tag{B11}$$

$$\frac{\partial N^{\text{eff}}_{X\sigma}}{\partial x_\sigma} = S_{N\sigma}\left(\frac{2}{3}\right)^{3/2} \frac{\pi\rho^{5/2}\mathrm{e}^{x_\sigma}}{x_\sigma^2 Q_\sigma}\sqrt{\frac{x_\sigma - 2}{x_\sigma\, Q_\sigma}}\left(x_\sigma^2 - 2x_\sigma + 3\right). \tag{B12}$$

Here, $S_{N\sigma}$ is a factor related to the smoothening of the upper limit $N^{\text{eff}}_{X\sigma} \le 2$, similar to $S_{f\sigma}$, Eq. (B9)

$$S_{N\sigma} = \begin{cases} 1, & N^{\text{eff}}_{X\sigma} \le (2-\delta_2) \\ -\dfrac{(N^{\text{eff}}_{X\sigma} - 2 - \delta_2)}{2\delta_2}, & (1-\delta_2) < N^{\text{eff}}_{X\sigma} < (1+\delta_2) \\ 0, & N^{\text{eff}}_{X\sigma} \ge (2+\delta_2) \end{cases} \qquad \delta_2 = 0.07. \tag{B13}$$

The derivatives $\frac{dx_\sigma}{dy_\sigma}$ here and further on are used in the analytic form of Eqs. (31), (36), and (40)

$$y_\sigma = -\frac{3}{4\pi}\frac{Q_\sigma}{\rho_\sigma^2} U^{\text{ex}}_{X\sigma},$$

$$\frac{\partial y_\sigma}{\partial \rho_\sigma} = \frac{U^{\text{ex}}_{X\sigma}}{4\pi\rho_\sigma^3}\left(9Q_\sigma + \frac{|\nabla\rho_\sigma|^2}{4\rho_\sigma}\right), \tag{B14}$$

$$\frac{\partial N^{\text{eff}}_{X\sigma}}{\partial Q_\sigma} = -S_{N\sigma}\frac{3}{2Q_\sigma}\left(\frac{2}{3}\right)^{3/2} \pi\rho_\sigma^{5/2} e^{x_\sigma}\left[\frac{(x_\sigma - 2)}{x_\sigma\, Q_\sigma}\right]^{3/2}, \tag{B15}$$

$$\frac{\partial Q_\sigma}{\partial \rho_\sigma} = -\frac{|\nabla\rho_\sigma|^2}{12\rho_\sigma}. \tag{B16}$$

Next, we consider the derivative of $N^{\text{eff}}_{X\sigma}$ over the functional variable, $\gamma_\sigma \equiv (\nabla\rho_\sigma)^2$,

$$\frac{dN^{\text{eff}}_{X\sigma}}{d\gamma_\sigma} = \frac{\partial N^{\text{eff}}_{X\sigma}}{\partial x_\sigma}\frac{dx_\sigma}{dy_\sigma}\frac{\partial y_\sigma}{\partial \gamma_\sigma} + \frac{\partial N^{\text{eff}}_{X\sigma}}{\partial Q_\sigma}\frac{\partial Q_\sigma}{\partial \gamma_\sigma}, \tag{B17}$$

$$\frac{\partial y_\sigma}{\partial \gamma_\sigma} = -\frac{U^{\text{ex}}_{X\sigma}}{16\pi\rho_\sigma^3}, \tag{B18}$$

$$\frac{\partial Q_\sigma}{\partial \gamma_\sigma} = \frac{1}{12\rho_\sigma}. \tag{B19}$$

Next is the derivative of $N^{\text{eff}}_{X\sigma}$ over the kinetic energy density, τ_σ,

$$\frac{dN^{\text{eff}}_{X\sigma}}{d\tau_\sigma} = \frac{\partial N^{\text{eff}}_{X\sigma}}{\partial x_\sigma}\frac{dx_\sigma}{dy_\sigma}\frac{\partial y_\sigma}{\partial \tau_\sigma} + \frac{\partial N^{\text{eff}}_{X\sigma}}{\partial Q_\sigma}\frac{\partial Q_\sigma}{\partial \tau_\sigma}, \tag{B20}$$

$$\frac{\partial y_\sigma}{\partial \tau_\sigma} = -\frac{U_{X\sigma}^{\rm ex}}{4\pi\rho_\sigma^2}, \quad \frac{\partial Q_\sigma}{\partial \tau_\sigma} = -\frac{1}{3}. \tag{B21}$$

The derivative of $N_{X\sigma}^{\rm eff}$ over the Laplacian variable $\nabla^2\rho_\sigma$ reads

$$\frac{dN_{X\sigma}^{\rm eff}}{d(\nabla^2\rho_\sigma)} = \frac{\partial N_{X\sigma}^{\rm eff}}{\partial x_\sigma}\frac{dx_\sigma}{dy_\sigma}\frac{\partial y_\sigma}{\partial(\nabla^2\rho_\sigma)} + \frac{\partial N_{X\sigma}^{\rm eff}}{\partial Q_\sigma}\frac{\partial Q_\sigma}{\partial(\nabla^2\rho_\sigma)}, \tag{B22}$$

$$\frac{\partial y_\sigma}{\partial(\nabla^2\rho_\sigma)} = -\frac{U_{X\sigma}^{\rm ex}}{8\pi\rho_\sigma^2}, \quad \frac{\partial Q_\sigma}{\partial(\nabla^2\rho_\sigma)} = \frac{1}{6}. \tag{B23}$$

The list of derivatives for the opposite-spin ND component ends with the derivative of $N_{X\sigma}^{\rm eff}$ over the exact exchange energy density $V_{X\sigma}^{\rm ex}$

$$\frac{dN_{X\sigma}^{\rm eff}}{dV_{X\sigma}^{\rm ex}} = -\frac{\partial N_{X\sigma}^{\rm eff}}{\partial x_\sigma}\frac{dx_\sigma}{dy_\sigma}\left(\frac{3Q_\sigma}{4\pi\rho_\sigma^3}\right). \tag{B24}$$

Turning now to the same-spin ND component of the KS potential matrix, Eq. (52), the derivatives that are required are listed below

$$\frac{dA_{1\sigma}}{d\xi_\sigma} = -\frac{1}{M_\sigma^{(2)}}\left[\frac{dN_{X\sigma}^{\rm eff}}{d\xi_\sigma} + N_{X(-\sigma)}^{\rm eff}\frac{df}{d\xi_\sigma}\right] - \frac{1}{\left(M_\sigma^{(2)}\right)^2}\frac{dM_\sigma^{(2)}}{d\xi_\sigma}\left(1 - N_{X\sigma}^{\rm eff} - f\,N_{X(-\sigma)}^{\rm eff}\right), \tag{B25}$$

$$\frac{dA_{1\alpha}}{d\xi_\beta} = -\frac{1}{M_\alpha^{(2)}}\left[f\frac{dN_{X\beta}^{\rm eff}}{d\xi_\beta} + N_{X\beta}^{\rm eff}\frac{df}{d\xi_\beta}\right], \tag{B26}$$

$$\frac{dM_\sigma^{(l)}}{d\rho_\sigma} = \frac{\partial M_\sigma^{(l)}}{\partial\rho_\sigma} + \frac{\partial M_\sigma^{(l)}}{\partial x_\sigma}\frac{dx_\sigma}{dy_\sigma}\frac{\partial y_\sigma}{\partial\rho_\sigma} + \frac{\partial M_\sigma^{(l)}}{\partial Q_\sigma}\frac{\partial Q_\sigma}{\partial\rho_\sigma},\ l \equiv 1,\ \text{or}\ 2, \tag{B27}$$

$$\frac{dM_\sigma^{(l)}}{d\xi_\sigma} = \frac{\partial M_\sigma^{(l)}}{\partial x_\sigma}\frac{dx_\sigma}{dy_\sigma}\frac{\partial y_\sigma}{\partial\rho_\sigma} + \frac{\partial M_\sigma^{(l)}}{\partial Q_\sigma}\frac{\partial Q_\sigma}{\partial\rho_\sigma}, \quad \xi_\sigma \equiv (\nabla\rho_\sigma)^2,\ \tau_\sigma,\ \text{or}\ \nabla^2\rho_\sigma, \tag{B28}$$

$$\frac{dM_\sigma^{(l)}}{dV_{X\sigma}^{\rm ex}} = \frac{\partial M_\sigma^{(l)}}{\partial x_\sigma}\frac{dx_\sigma}{dy_\sigma}\frac{\partial y_\sigma}{\partial V_{X\sigma}^{\rm ex}}. \tag{B29}$$

$$\frac{\partial M_\sigma^{(1)}}{\partial\rho_\sigma} = \frac{3}{\rho_\sigma}M_\sigma^{(1)}, \tag{B30}$$

$$\frac{\partial M_\sigma^{(1)}}{\partial Q_\sigma} = -\frac{2}{Q_\sigma}M_\sigma^{(1)},$$

$$\frac{\partial M_\sigma^{(1)}}{\partial x_\sigma} = \frac{2\pi\rho_\sigma^3(x_\sigma-2)}{9x_\sigma^4 Q_\sigma^2} \times\left[e^{x_\sigma}\left(x_\sigma^4 - x_\sigma^3 + 6x_\sigma^2 - 12x_\sigma + 24\right) - 24\right], \tag{B31}$$

$$\frac{\partial M_\sigma^{(2)}}{\partial\rho_\sigma} = \frac{7}{2\rho_\sigma}M_\sigma^{(2)}, \tag{B32}$$

$$\frac{\partial M_\sigma^{(2)}}{\partial Q_\sigma} = -\frac{5}{2Q_\sigma}M_\sigma^{(2)}, \tag{B33}$$

$$\frac{\partial M_\sigma^{(2)}}{\partial x_\sigma} = \frac{\pi\rho_\sigma^3\sqrt{6}(x_\sigma-2)}{27x_\sigma^3 Q_\sigma^2}\sqrt{\frac{\rho_\sigma(x_\sigma-2)}{x_\sigma Q_\sigma}} \times e^{x_\sigma}\left[x_\sigma^4 + 13x_\sigma^2 - 24x_\sigma + 60\right], \tag{B34}$$

$$\frac{\partial A_{2\sigma}}{\partial\rho_\sigma} = -\frac{\tau_\sigma}{3\rho_\sigma^2} + \frac{(\nabla\rho_\sigma)^2}{6\rho_\sigma^3}, \tag{B35}$$

$$\frac{\partial A_{2\sigma}}{\partial\left((\nabla\rho_\sigma)^2\right)} = -\frac{1}{12\rho_\sigma^2}, \tag{B36}$$

$$\frac{\partial A_{2\sigma}}{\partial\tau_\sigma} = \frac{1}{3\rho_\sigma}, \tag{B37}$$

$$\frac{\partial A_{2\sigma}}{\partial(\nabla^2\rho_\sigma)} = 0, \quad \frac{\partial A_{2\sigma}}{\partial V_{X\sigma}^{\rm ex}} = 0. \tag{B38}$$

Considering the derivatives of the functional variables over $P_{\mu\nu}^\alpha$ that are required to complete the evaluation of the potential matrix, Eq. (48), special attention should be paid to the derivative of the exact exchange energy density

$$\frac{\partial V_X^{\rm HF}(\mathbf{r})}{\partial P_{\mu\nu}} = -2\sum_{m,n}V_{mn}(\mathbf{r})\sum_i C_m^{i\mu}C_n^{i\nu}, \quad C_m^{i\mu} = \sum_\lambda C_{i\lambda}C_m^{\lambda\mu}, \tag{B39}$$

where $C_m^{i\mu}$ is the half-transform of the RI fitting coefficient matrix from Eq. (57). The second sum in Eq. (B39) above, involves 5 orbital indices, which makes the overall cost as $O(N_B^5)$. To reduce this cost, we first combine together the ND terms of the KS matrix in the form

$$F_{\mu\nu}^{{\rm nd},\sigma} = F_{\mu\nu}^{{\rm nd\text{-}op},\sigma} + F_{\mu\nu}^{{\rm nd\text{-}par},\sigma} = \left(\sum_{\xi\neq(V_{X\alpha}^{\rm HF},V_{X\beta}^{\rm HF})}\int S(\xi(\mathbf{r}))\frac{\partial\xi(\mathbf{r})}{\partial P_{\mu\nu}^\sigma}d\mathbf{r}\right) + \int Q^\sigma(\mathbf{r})\frac{\partial V_{X\sigma}^{\rm ex}(\mathbf{r})}{\partial P_{\mu\nu}^\sigma}d\mathbf{r}, \tag{B40}$$

where the factors $S(\xi)$ and Q^σ can be deduced directly from Eqs. (51) and (52). Then, the second integral on the rhs above is expressed as

$$\int Q(\mathbf{r})\frac{\partial V_X^{\rm HF}(\mathbf{r})}{\partial P_{\mu\nu}}d\mathbf{r} = -\sum_{i,m}C_m^{i\mu}\sum_n C_n^{i\nu}\int Q(\mathbf{r})(V_{mn}(\mathbf{r}) + V_{nm}(\mathbf{r}))\,d\mathbf{r}. \tag{B41}$$

The numerical integration here costs as $O(N_G N_B^2)$ and the two summations are of $O(N_B^4)$. In our code, first the numerical integration is done to form the matrices in the auxiliary basis. Then the transformation to the atomic basis is done after the loop of all the grid batches is over. Again, the matrix in the auxiliary basis V needs to be symmetrized (see Eq. (60)).

APPENDIX C: LIST OF OUR ATOMIZATION ENERGY TEST SET

The set of atomization energies (in eV) of 26 diatomic and 43 polyatomic molecules calculated with the re-optimized SCF-RI-B05 of this work.

26 Diatomic	Calculated	Exact	Deviation	43 Polyatomics	Calculated	Exact	Deviation
H_2	4.7368	4.7500	−0.0132	HCN	13.5121	13.5700	−0.0579
N_2	9.6831	9.9100	−0.2269	H_2O	10.0038	10.0900	−0.0862
F_2	1.7249	1.6600	0.0649	H_2S	7.9033	7.9200	0.0167
O_2	4.9227	5.2100	−0.2873	CO_2	16.9925	16.8700	0.1225
S_2	4.3556	4.4100	−0.0544	NH_3	12.8333	12.9200	−0.0867
P_2	5.2282	5.0800	0.1482	PH_3	10.6349	10.4700	0.1649
Cl_2	2.5573	2.5100	0.0473	N_2O	11.6896	11.7300	−0.0404
HF	6.1736	6.1200	0.0536	H_2O_2	11.5067	11.6500	−0.1433
CO	11.200	11.2400	−0.0400	SiH_4	14.1215	13.9800	0.1415
NO	6.3790	6.5900	−0.2110	CH_4	18.2513	18.2200	0.0313
PN	6.3086	6.2200	0.0886	C_2H_2	17.5997	17.5800	0.0197
CN	7.5735	7.8300	−0.2565	C_2H_4	24.4754	24.4400	0.0354
NH	3.6114	3.6300	−0.0186	C_2H_6	30.7389	30.9100	−0.1711
CS	7.3642	7.4300	−0.0658	H_2CO	16.2468	16.2100	0.0368
CH	3.6496	3.6400	0.0096	CH_3OH	22.1778	22.2500	−0.0722
OH	4.5656	4.6400	−0.0744	CH_2OH	17.6690	17.7700	−0.1010
HCl	4.6229	4.6100	0.0129	C_6H_6	59.2513	59.3000	−0.0487
SiO	8.4247	8.3300	0.0947	C_4H_6	43.9086	43.9000	0.0086
ClF	2.7899	2.6700	0.1199	C_4H_5N	46.3555	46.4700	−0.1145
ClO	2.7372	2.8000	−0.0628	C_5H_5N	53.6357	53.6700	−0.0343
Li_2	1.0193	1.1400	−0.1207	$AlCl_3$	13.2821	13.2800	0.0021
LiF	6.3236	6.0100	0.3136	BCl_3	14.0083	14.0000	−0.0083
LiH	2.6271	2.5200	0.1071	BF_3	20.7743	20.3800	0.3943
MgS	2.2333	2.0300	0.2033	C_2Cl_4	20.1140	20.2200	−0.1060
Si_2	3.2229	3.2500	−0.0271	C_2H_4O	28.1598	28.2200	−0.0602
SO	5.2686	5.4300	−0.1614	CCH	11.4814	11.5000	−0.0186
	MAE		0.1109 eV	CCl_4	13.2567	13.5600	−0.3033
			2.56 kcal/mol				
				CF_4	20.8599	20.6500	0.2099
				CH_{2a}	7.8052	7.8600	−0.0548
				CH_{2b}	8.4230	8.2700	0.1530
				CH_3Cl	17.1183	17.1500	−0.0317
				CH_3CN	26.6671	26.7000	−0.0329
				CH_3CO	25.1965	25.2200	−0.0235
				CH_3NH_2	25.1165	25.2600	−0.1435
				CH_3NO_2	25.9711	26.0700	−0.0989
				CH_3SH	20.4914	20.5500	−0.0586
				CHF_3	20.0803	19.8400	0.2403
				HCO	12.0752	12.0700	−0.0052
				N_2H_4	18.7976	19.0200	−0.2224
				Si_2H_6	23.1739	23.1800	−0.0061
				SiH_{2a}	6.7461	6.5800	0.1661
				SiH_{2b}	5.7521	5.6800	0.0721
				SO_2	11.0995	11.2100	−0.1105
					MAD		0.0943 eV
							2.18 kcal/mol

[1]A. D. Becke, J. Chem. Phys. **119**, 2972 (2003).
[2]J. P. Perdew, V. N. Staroverov, J. Tao, and G. E. Scuseria, Phys. Rev. A **78**, 052513 (2008).
[3]M. Weimer, F. D. Sala, and A. Gorling, J. Chem. Phys. **128**, 144109 (2008).
[4]E. J. Baerends, Phys. Rev. Lett. **87**, 133004 (2001).
[5]J. W. Hollett and P. M. W Gill, J. Chem. Phys. **134**, 114111 (2011).
[6]J. Toulouse, P. Gori-Giorgi, and A. Savin, Theor. Chem. Acc. **114**, 305 (2005).

[7]A. D. Becke, J. Chem. Phys. **122**, 64101 (2005).
[8]P. Gori-Giorgi, M. Seidl, and G. Vignale, Phys. Rev. Lett. **103**, 166402 (2009).
[9]A. J. Cohen, P. Mori-Sanchez, and W. Yang, Science **321**, 792 (2008).
[10]P. Gori-Giorgi and M. Seidl, Phys. Chem. Chem. Phys. **12**, 14405 (2010).
[11]D. H Ess, E. R. Johnson, X. Hu, and W. Yang, J. Phys. Chem. A **115**, 76 (2011).
[12]A. J. Cohen, P. Mori-Sanchez, and W. Yang, J. Chem. Phys. **129**, 121104 (2008).
[13]A. Ruzsinszky, J. P. Perdew, and G. I. Csonka, J. Chem. Phys. **124**, 114110 (2011).
[14]R. M. Dickson and A. D. Becke, J. Chem. Phys. **123**, 111101 (2005).
[15]A. V. Arbuznikov and M. Kaupp, J. Chem. Phys. **131**, 084103 (2009).
[16]E. Proynov, Y. Shao, and J. Kong, Chem. Phys. Lett. **493**, 381 (2010).
[17]Y. Zhao and D. G. Truhlar, Theor. Chem. Acc. **120**, 215 (2008).
[18]B. J. Lynch and D. G. Truhlar, J. Phys. Chem. A **107**, 3898 (2003).
[19]N. Neshev, E. Proynov, and T. Mineva, Bulg. Chem. Commun. **30**, 488 (1998).
[20]A. D. Becke, Int. J. Quant. Chem. Symp. **28**, 625 (1994).
[21]E. Proynov, Z. Gan, and J. Kong, Chem. Phys. Lett. **455**, 103 (2008).
[22]A. D. Becke and M. R. Roussel, Phys. Rev. A **39**, 3761 (1989).
[23]A. V. Arbuznikov and M. Kaupp, J. Mol. Struct.: THEOCHEM **762**, 151 (2006).
[24]J. P. Perdew and K. Schmidt, in *Density Functional Theory and its Application to Materials*, edited by V. Van Doren, C. Van Alsenoy, and P. Geerkings (AIP, Melville, NY, 2001).
[25]J. P. Perdew and J. Tao, J. Mol. Struct.: THEOCHEM **943**, 19 (2010).
[26]J. Kong, E. Proynov, and Y. Shao, "Real-space correlation methods of describing nondynamic correlation in DFT," Q-Chem Project Report (2007).
[27]E. Proynov and J. Kong, J. Chem. Theory Comput. **3**, 746 (2007).
[28]R. Neumann, H. Nobles, and N. C. Handy, Mol. Phys. **87**, 1 (1996).
[29]B. G. Janesko, A. V. Krukau, and G. E. Scuseria, J. Chem. Phys. **129**, 124110 (2008).
[30]Y. Jung, A. Sodt, P. M. W. Gill, and M. Head-Gordon, Proc. Natl. Acad. Sci. U.S.A. **102**, 6692 (2005).
[31]Y. Shao, L. Fusti-Molnar, Y. Jung, J. Kussmann, C. Ochsenfeld, S. T. Brown, A. T. B. Gilbert, L. V. Slipchenko, S. V. Levchenko, D. P. O'Neill, R. A. DiStasio Jr, R. C. Lochan, T. Wang, G. J. O. Beran, N. A. Besley, J. M. Herbert, C. Yeh Lin, T. Van Voorhis, S. H. Chien, A. Sodt, R. P. Steele, V. A. Rassolov, P. E. Maslen, P. P. Korambath, R. D. Adamson, B. Austin, J. Baker, E. F. C. Byrd, H. Dachsel, R. J. Doerksen, A. Dreuw, B. D. Dunietz, A. D. Dutoi, T. R. Furlani, S. R. Gwaltney, A. Heyden, S. Hirata, C.-P. Hsu, G. Kedziora, R. Z. Khalliulin, P. Klunzinger, A. M. Lee, M. S. Lee, W. Liang, I. Lotan, N. Nair, B. Peters, E. I. Proynov, P. A. Pieniazek, Y. Min Rhee, J. Ritchie, E. Rosta, C. D. Sherrill, A. C. Simmonett, J. E. Subotnik, H. L. Woodcock III, W. Zhang, A. T. Bell, A. K. Chakraborty, D. M. Chipman, F. J. Keil, A. Warshel, W. J. Hehre, H. F. Schaefer III, J. Kong, A. I. Krylov, P. M. W. Gill, and M. Head-Gordon, Phys. Chem. Chem. Phys. **8**, 3172 (2006).
[32]L. A. Curtiss, K. Raghvachari, P. C. Redfern, V. Rassolov, and J. A. Pople, J. Chem. Phys. **109**, 7764 (1998).
[33]E. Proynov and J. Kong, in *Theoretical Aspects of Catalysis*, edited by G. Vayssilov and T. Mineva (Heron Press, Sofia, 2008), p. 453.
[34]Y. Zhao and D. G. Truhlar, J. Phys. Chem. A **110**, 13126 (2006).
[35]Y. Zhao and D. G. Truhlar, J. Chem. Phys. **125**, 194101 (2005).
[36]H. A Duarte, E. Proynov, and D. R. Salahub, J. Chem. Phys. **109**, 26 (1998).
[37]R. Gonzalez-Luque, M. Merchan, and B. O. Roos, Theor. Chim. Acta **88**, 425 (1994).
[38]A. L. L. East, J. Chem. Phys. **109**, 2185 (1998).
[39]S. V. Levchenko, H. Reisler, A. I. Krylov, O. Gessner, A. Stolow, H. Shi, and A. L. L. East, J. Chem. Phys. **125**, 084301 (2006).
[40]N. Taguchi, Y. Mochizuki, T. Ishikawa, and K. Tanaka, Chem. Phys. Lett. **451**, 31 (2008).
[41]B. J. Howard and A. R. W. McKellar, Mol. Phys. **78**, 55 (1993).
[42]J. R. Hetzler, M. P. Casassa, and D. S. King, J. Chem. Phys. **95**, 8086 (1991).